Experimental investigations of three laser-induced synchronized bubbles

Hengzhu Bao, Hongchao Zhang, Lou Gao, Mao Tang, Chong Zhang, Jian Lu [*]

School of Science, Nanjing University of Science and Technology, China

ARTICLE INFO

ABSTRACT

Herein, we investigated experimentally the dynamics of three laser-induced, same-sized, symmetrically aligned, and synchronized bubbles. Three synchronized laser beams split from the same beam using a Diffractive Optical Element splitter were focused on water, and then we obtained three bubbles. Another nanosecond laser pulse was used to probe the bubbles to obtain shadowgraphs. The exact delay of the excited and detected light was controlled using a delay generator. The results revealed that the maximum volumes of bubbles in arrays decrease as the normalized distance falls, while the lifetimes and translation increase. It was explained by the interaction between the acoustic radiation of bubbles and the surrounding bubbles. The shrinkage of linear bubble arrays exists an anomaly. The center bubbles were stretched, to ellipsoid, stick, even fractured, by the peripheral bubbles. The closer they are, the more distinct is the above phenomenon. However, when the normalized distance was sufficiently small, instead of being stretched, the center bubbles were compressed to disk shape and thus shrank with the whole array. Finally, the dependence of the distance on the energy transfer of the bubble system is also discussed.

1. Introduction

Cavitation is an important phase-transition phenomenon in many fields, such as acoustics, sonochemistry, medicine, and hydraulics [1–8]. In the practice of these fields, cavitation is not isolated single one but tends to appear as filaments, streamers, clusters, and clouds in different styles of multiple bubbles groups. Studies on cavitation mainly focus on the deformation and mechanics revealed in the bubble dynamics and also the primary parameters of which are the phase and the size of bubbles. In a tiny region of the bubble groups, every two adjacent bubbles usually have similar phases and sizes [1,9,10]. In this respect, it is thus critical to clarify the interaction among the same-sized and synchronized multiple bubbles.

Many previous studies have focused on a single bubble, which assumes that the individual bubble behaviors are independent of the groups. The dynamics of a single bubble has been studied extensively for many years. For instance, Rayleigh, Plesset, Gilmore, and Keller studied the aspects of a single spherical bubble and developed the corresponding mathematical models [11–18]. On the other hand, in the studies of bubble groups, it was assumed that all bubbles followed the Rayleigh-Plesset model. In this case, these bubbles oscillate with the driving acoustic fields. Moreover, the natural frequency of bubble groups is lower than that of a single bubble. In the center of bubble groups, there exists energy accumulation and radiates high-intensity noise. When generated near the rigid boundary, bubble groups keep stationary for a while and then move toward the rigid boundary [7,18–27].

In fact, each bubble in the bubble groups is not independent. Thus the investigations on the interaction between two bubbles are significant because such studies can provide a valuable basis for multiple bubbles. Shima, Prosperetti, Mettin, Harkin, Fujikawa, Lauternborn, B.C. Khoo, Ohl explored two bubbles experimentally and theoretically based on the hypothesis of bubbles keeping spherical [28–37]. Consequently, it was noted that two synchronized bubbles with similar sizes usually attract each other and form jets towards each other in their shrink phase, and they have a longer lifetime. Nonetheless, when bubble pairs only have one pair of interactions, while bubbles in groups usually have several adjacent bubbles to interact with. Furthermore, the exact mechanism of interaction among multiple (i.e., three or more) bubbles remains elusive [1,38]. However, the studies of bubble arrays have partially solved this problem.

Elsewhere, J.P.Dear and J.E.Field created static tension bubbles in gelatin, to study the reaction of acoustic pulse on the bubble arrays [39,40]. Nicolas Bremond, Manish Arora, Claus-Dieter Ohl, and Detlef Lohse studied the interaction of inflatable bubble arrays generated from a rigid surface [41,42]. Quinto-Su, Claus-Dieter Ohl focused laser modified by a spatial light modulator (SLM) on a liquid gap clamped by

---

glass slides, to obtain quasi-two-dimensional bubble arrays. The studies indicated that, for a specific bubble, its adjacent bubbles modify its ambient pressure, and thereby mutually screen the pressure from the further position at the direction of the adjacent bubble [40,43]. The inner bubbles are confined by adjacent bubbles in the array dimensions. Their dynamics are primarily controlled by the reaction of adjacent bubbles and the free dimension. On the other hand, the peripheral bubbles are minimally confined, and their lifetimes are close to the isolated single bubble. Hence, the bubbles located centrally live most. Then the arrays collapse with a time sequence from outer to inner.

In general, three bubbles should receive more attention due to their high observability caused by a little amount, and high representativeness of mutual interaction from multiple adjacent bubbles. Siew-Wan Ohl, Lup Wai Chew, B.C. Khoo, and A.M. Zhang studied the dynamics of arrays of three bubbles generated by electric sparks in the free domain [34,36,44]. When the distances between synchronized bubbles are large, the center bubble will split when collapse, and each part will join with the verge bubbles, whereas three bubbles will join directly in the small distance case. The generated time and size influence the direction and style of bubble collapse. However, they did not control the position and energy of the exciting sources orderly. The dependence of separate distance on the orderly arranged arrays of similar bubbles has yet to be fully revealed.

In this paper, the holographic generation of millimeter-sized bubbles in a three-dimensional water column is attained using a high-power laser with a splitter. We used three split laser beams to accurately generate synchronized bubbles, with strictly controlled initial phases and size. Herein we purposed to clarify the dynamics of linear arrays of same-sized and synchronized cavitation bubbles in a quasi-free domain. Note that this paper concentrates on the deformation, size, lifetime, and translation of three synchronized bubbles in uniform alignment at different separate distances, during the period from birth to collapse, of laser-induced cavitation bubbles, which differs from the investigations above. Our approach is suitable for 3D geometries and a rather high laser fluence, which previously were not available. Such a study is currently lacking, and thus there is an urgent need for this aspect to be probed.

This paper is structured as follows. The second chapter introduces the experimental arrangement and the parameters of measurement. Relevant experimental results are presented in Chapter 3. In this chapter, the dynamics of multiple bubbles in the first oscillation period are analyzed. Then in a new chapter, some further discussions on the experiments are stated. Finally, minimum conclusions are provided.

2. Experimental setup

The experimental arrangement employed in this study for investigating the dynamics of laser-induced three symmetrically aligned in-phase bubbles is depicted in Fig. 1.

To generate cavitation bubbles, a pulsed Nd:YAG laser generator (wavelength:1064 nm; maximum energy:1J; pulse duration:10 ns) was employed. The single laser pulse energy ranges from 100 mJ to 1 J. The fluctuations of the laser energy are approximately ± 5%. Additionally, a beam splitter was utilized to split the pulse into two parts. Of which one part was reflected in an energy meter to monitor the incident pulse energy, while the other part was modulated into three beams using a triple-spot splitter DOE (Diffractive Optical Element; Holo/Or TS-245-I-Y-A). These three beams were aligned in the same vertical plane. Three mirrors were utilized to reflect these beams to an aplanat (f = 30 mm). The three reflecting spots aligned in the intersection of the incident plane, and also the plane in which the reflected laser and alignment bubbles were. Afterward, the aplanat lens was used for focusing on smaller spots to obtain regular bubbles. Hence, three pulse beams were focused and aligned on the focal plane. At these three focal points, deionized water was broken down in the water tank (fused silica, 50 mm* 50 mm * 50 mm). Furthermore, plasma was generated, which then evolved into bubbles. We can obtain one or two bubbles by blocking certain beams. During the experiments, we set the different angles of the three incident beams, and the different distance between the mirrors to get different distances of the foci.

To visualize the fast process of bubble oscillation, we used a single frame CCD(Imi,imc7017g) combined with a short duration laser (Nd: YAG, wavelength = 1064 nm, pulse duration = 2.5 ns). The probe laser propagates through the KTP frequency doubling crystal, and then the 1064 nm pulse is transformed into a 532 nm pulse. The new probe pulse beam was decayed and expanded through the aperture and the collimating expanding lens system. Afterward, the pulse beam which carries the information of bubbles propagates in the water and then approaching the CCD camera. The detection light was perpendicular to the exciting laser and the bubble line. A delay generator (Stanford Research Systems Inc., DG535) was utilized to trigger the CCD camera and lasers. By reading the time delay between the plasma flash and probe pulse, which was detected by a photodiode, we obtained the exact time of the image which was gathered using the CCD.

Here, parameters that we focused on include the size and distance of bubbles. The radii of bubbles at a specific time, R, are obtained by the shadows, whose area is πR^2. Given is the maximum radius of bubbles R_0 in a single oscillation process. The initial distance D_0 is the mean value of
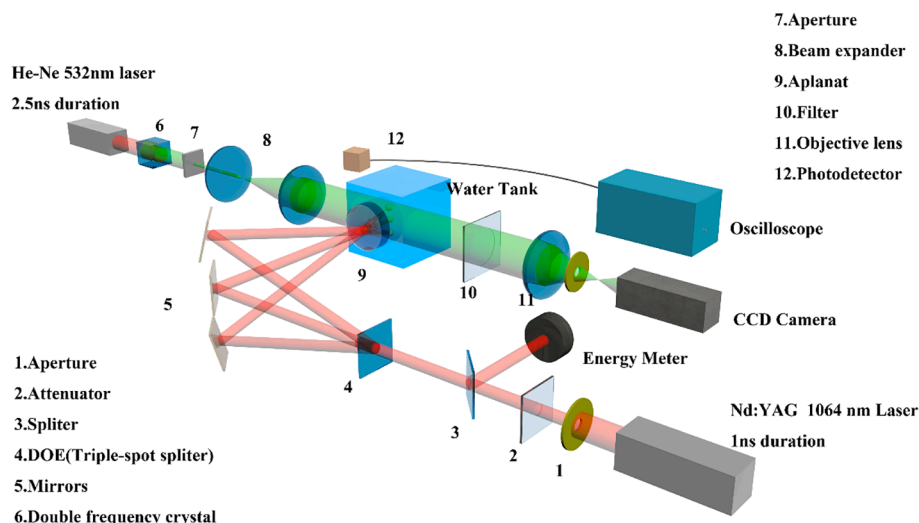

Fig. 1. Experimental arrangement for shadowgraphy of laser-induced multiple cavitation bubbles.

the distances between each two adjacent breakdown spots, as depicted in Fig. 2. For normalization, a dimensionless parameter γ is defined as follows:

$$\gamma = \frac{D_0}{2R_0} \tag{1.1}$$

Other important parameters in the bubble dynamics A, B are shown in Fig. 2. Because of the interaction between bubbles, they lose their sphericities during the oscillation. Considering two-dimensional patterns, A is the semi-major axis of the bubble in the photos, while B is the semi-minor axis. However, the profile of the bubble is usually irregular. We treat the horizontal axis of the minimum bounding rectangle as the major axis of the bubble. Moreover, the distance from the centroid to the outer horizontal side of the rectangle is defined as the B-outer, so does the B-inner. Two verge/peripheral bubbles average a general A, B-outer, and B-inner. Furthermore, B of the center bubble is the average of the distances from the centroid to the top and bottom.

To understand the deformation in the whole process, a normalized parameter C, that is, the degree of circularity is introduced [45]. It is defined as follows:

$$C = \frac{\text{perimeter of area - equivalent circle}}{\text{perimeter of bubble}} = \frac{2\sqrt{\pi S}}{P_b}, \tag{1.2}$$

where S denotes the area of the bubble in the photos, which has a perimeter P_b. The numerator of this equation means the perimeter or circumference of a circle, which has an area equal to that of a bubble with perimeter P_b. In this case, a perfect circle has a $C = 1$. The more the bubble shape varies from being a circle, the smaller the circularity value.

To track the relative location changing of bubbles, a non-dimensional distance $\tilde{D}$ is introduced. It is defined as follows:

$$\tilde{D} = \frac{D}{D_0}, \tag{1.3}$$

where D represents the distance in a certain time, while D_0 represents the initial distance between the verge bubbles to the center bubble as introduced in Fig. 2.

In these experiments, the maximum bubble radii were obtained in single spherical bubble experiments in the bulk of water before the bubble arrays experiments with the same laser energy [33,34]. We recorded the oscillation of single bubbles in bulk water as well as measured their collapse time. The results of this experiment concurred with the radius in the Keller-Miksis model. The time of collapse the photos recorded fluctuated about $\pm 5\%$. Thus, the ideal maximum radius of a single oscillating bubble in bulk water with a notation R_0 is characterized by the mid-value of collapse time [46]. Compared with the results from the area of shadows in the shadowgraph, which is $R_0 = (\sqrt{max(Area)})/\pi$, small differences can be ignored. The initial distance of bubbles, D_0, was extracted by the earliest frame below 100 ns, while plasma is recombining and converting to vapour [47].

Keller-Miksis(K-M) model is a relatively complete model, describing the oscillation of single spherical bubbles. It takes into account the surface tension, viscosity, compressibility and gas inside the bubble [17], reading

$$\left(1 - \frac{\dot{R}}{C}\right) R\ddot{R} + \frac{3}{2}\dot{R}^2 \left(1 - \frac{\dot{R}}{3c}\right) = \left(1 + \frac{\dot{R}}{C}\right) \frac{p_1}{\rho} + \frac{R}{\rho c} \frac{dp_1}{dt} \tag{1.4}$$

where R denotes the bubble's radius while ρ is the density of the liquid. Besides, the speed of sound in the liquid, C, is assumed to be a constant. The gas inside the bubble obeys the van der Waals law. Combined with the ambient pressure p_{stat}, the pressure at the bubble wall p_1 can be given as follows:

$$p_1 = \left(p_{stat} + \frac{2\sigma}{R_n}\right) \left(\frac{R_n^3 - bR_n^3}{R^3 - bR_n^3}\right)^{\kappa} - p_{stat} - \frac{2\sigma}{R} - \frac{4\mu}{R}\dot{R} - p(t) \tag{1.5}$$

where R_n is the equilibrium radius of the bubble, p_v is the vapor pressure, μ is the dynamic viscosity, and σ is the surface tension coefficient of the liquid, and $p(t)$ is the pressure of sound fields. Moreover, b is the van der Waals parameter given as 0.0016, while κ is the polytropic exponent denoted as 4/3. The concrete data used in calculations were retrieved from the references [46,48].

Herein, five groups of γ(0.45 = 1.35 mm/(2*1.5 mm), 0.80 = 2.40 mm/(2*1.5 mm), 1.0 = 3.0 mm/(2*1.5 mm), 1.47 = 2.94 mm/(2*1 mm), and 1.93 = 3.85 mm/(2*1 mm)) were employed for experimental studies. The aforementioned cases represent that the ideal geometry of adjacent bubbles is mutually covered, squeezed, touched, about, and aloof. Lastly, more than 20 photos were taken every 5 µs in the whole progress to assess the multi-bubbles dynamics for given conditions.

3. Experimental results

In this section, experimental results of typical cases and their mechanisms are interpreted based on the shadowgraph and the simplified explanation of bubble–bubble interaction. In particular, this only considers the effect of an acoustic pressure wave of a bubble radiated on the other bubbles [49–51]. The dominant parameter in this work is γ, the non-dimension distance between two adjacent bubbles, which is defined in formula 1.1.

Figs. 3, 5, 7, 9, 11 illustrates selected frames of the experimental photos of the dynamics of three symmetrical aligned in-phase bubbles
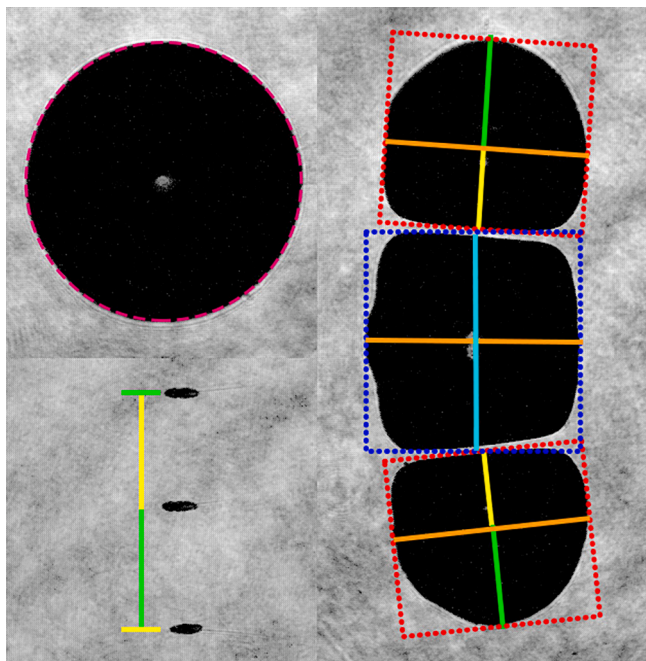

Fig. 2. A schematic description of the bubble setups, including the definitions of several essential parameters. The left upper frame shows the maximum radius of an isolated single bubble. The red dash is an outline circle. The shadow area can be used to calculate the radius, which is obtained by the collapse time with the K-M model. The left lower frame shows the initial breakdown spots when $\gamma = 0.45$. The mean value of the yellow and green length is the initial distance of bubbles, D_0. The right frame is a typical image in $\gamma = 0.8$. The red dash is the minimum bounding rectangle of the verge bubbles, whereas, the blue one is the minimum bounding rectangle of the center bubble. The green line is the B-verge-outer, while the yellow line is B-verge-inner. The pale blue line is the minor axis of the center bubble, B-center, while the orange line is the major axes, and also it can be defined as 2*A in different bubbles. D refers to the exact distance that is not shown in the scheme. It is a mean value of the distance of the centroids, which are the intersection points of the three cross in the frame. (For interpretation of the references to colour in this figure legend, the reader is referred to the web version of this article.)
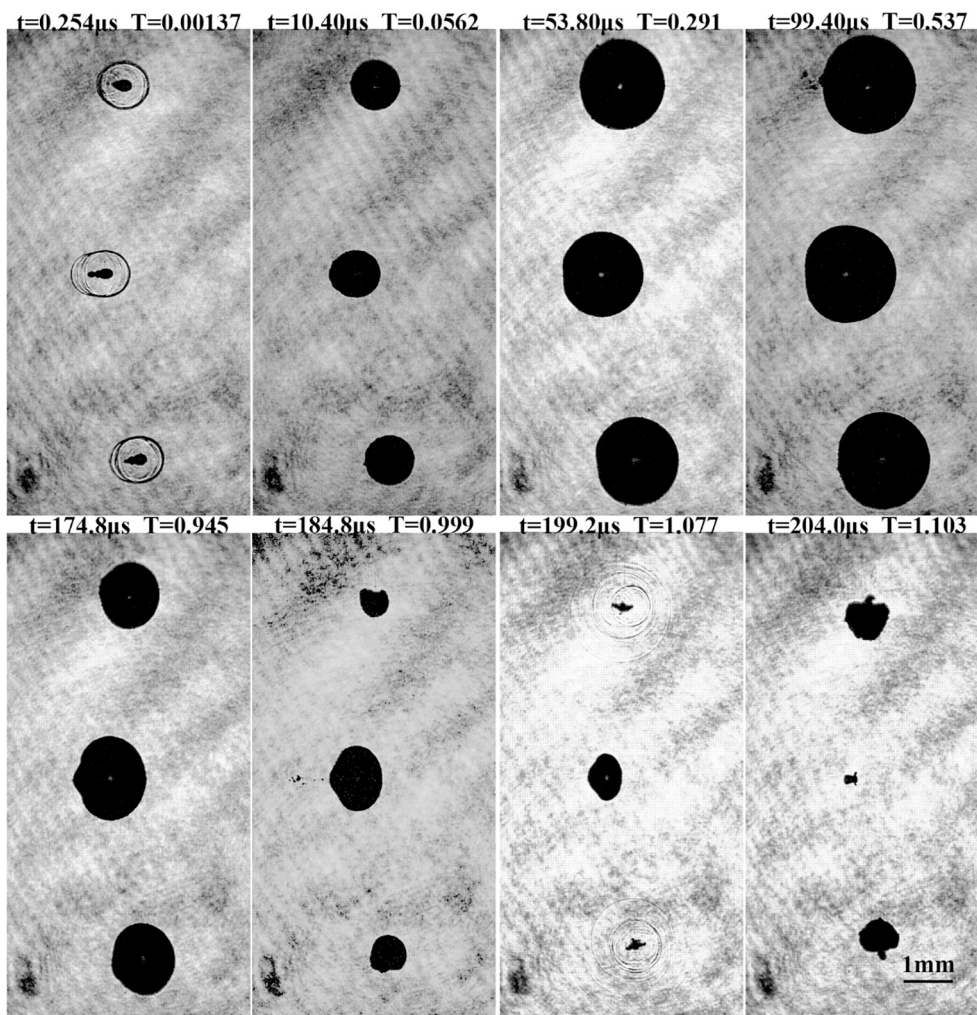
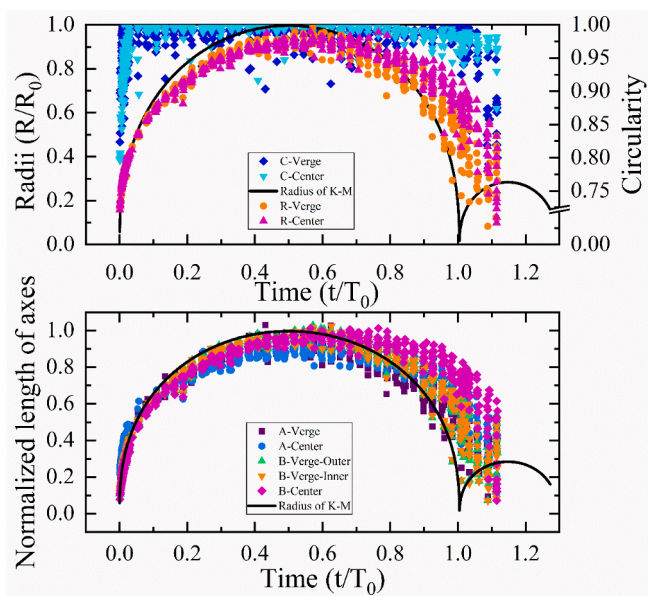**Fig. 3.** Case 1: Large γ ($\gamma = 1.93$) experimental results with the weakest interaction.

Fig. 4. Parameters in Case 1.

for five typical distances. The main process of Figs. 3–12 can be summarized as follows in terms of different values of γ and the relationship of the geometries of adjacent bubbles when they expand in isolation:

Case 1: Large γ ($\gamma = 1.93$ in Fig. 3), causes the isolated maximized geometries to leave each other. Two diameter-equaled space separated the bubbles at the maximum. They exhibited the weakest interaction in the experimental cases we have taken.

Case 2: Large γ ($\gamma = 1.47$ in Fig. 5), causes the isolated maximized geometries to near to each other. Two radius-equaled space separated the bubbles at the maximum. They elucidated the second weakest interaction in the experimental cases we have taken.

Case 3: Medium γ ($\gamma = 1.0$ in Fig. 7), causes the isolated maximized geometries to touch each other. The bubbles contacted to each other at the maximum radii and showed intermediate interaction in the experimental cases we have taken.

Case 4: Little γ ($\gamma = 0.80$ in Fig. 9), causes the isolated maximized geometries to squeeze each other. The bubbles contacted to each other before the maximum radii and had the second strongest interaction in the experimental cases we have taken.

Case 5: Little γ ($\gamma = 0.45$ in Fig. 11), causes the isolated maximized geometries to cover each other. The bubbles were quite close to each other, even have limited the early expanding significantly. In this case, bubbles had the strongest interaction in the experimental cases we have taken.

In the figures above and below (Fig. 3 – Fig. 13), t is the exact time and T_0 is the first oscillation period of bubbles in isolation, while $T = t/$
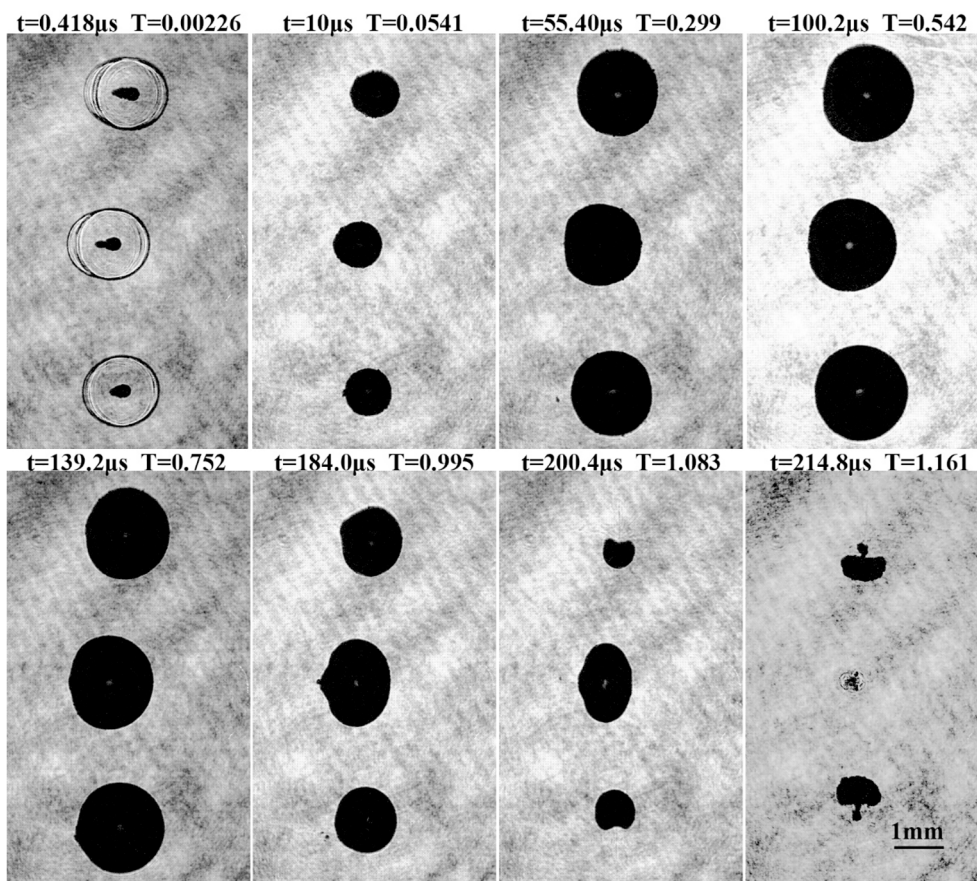
Fig. 5. Case 2: Large γ ($\gamma = 1.47$), experimental results with the second weakest interaction.
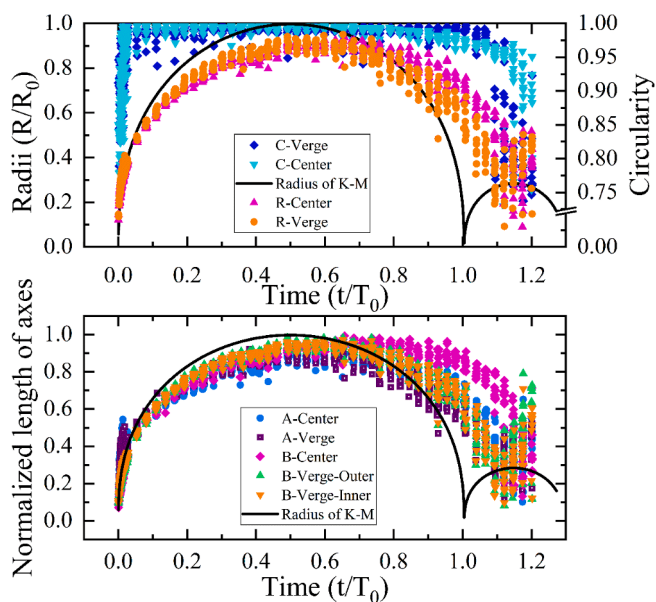

Fig. 6. Parameters in Case 2.

T_0 is the normalized time. Usually, an isolated bubble expands before $T = 0.5$, reaching its maximum at $T = 0.5$, then shrinks and eventually collapses at $T = 1$.

Figs. 3 and 4 display the results of Case 1, $\gamma = 1.93$. Big initial separations induce weak bubble interactions. In Fig. 3, the first frame reflects the starting of bubbles. The morphologies of bubbles nuclei are revealed to be similar to that of plasma calculated using a transient coupling model [47], which implies that this starting of bubbles follows the dynamics of the laser-induced plasma. Furthermore, based on the time series diagram, the deformation of the bubbles is primarily influenced by the initial shape. During the expansion period, the shadow area in frames 2, 3, 4 on the upper column, the volume of the center bubble was slightly smaller than that of the verge bubbles. This signifies that the phase of the center bubble is slightly delayed, and thus the verge bubbles reach the maximum bubble radius before the center one. Here, the phase was noted as the relative position of the bubbles' state of motion in a period, $\varphi = \pi(t_{exact}/T_{oscillation})$ [34]. If the period of periodic motion is extended, the time when a bubble reaches a certain phase is delayed. Here, phase delayed means that the period of the first oscillation is extended. In shrinkage, the phase of the verge bubbles also precedes the center bubble. The interactions caused by the pressure and tension waves of bubbles radiation are gradually becoming apparent. As indicated in the first frame of the bottom column, the bubbles elongated, and the outer edge of the verge bubbles get flattened and then shrink faster than the inner edge. Subsequently, as shown in the second frame of the bottom column, the verge bubbles produce jets pointing toward the center bubble, which remains a larger volume. In the third frame of the bottom column, the verge bubbles collapse and produce shock waves, but the center bubble survives and continues shrinking. Finally, the center bubble collapse after the fourth frame. Whilst, the positions of rebound verge bubbles move towards the center.

Fig. 4 depicts the normalized Rs and axes of bubbles and circularity over time. The distribution of Rs is flatter and wider compared to the K-M curve. This implies that the development of bubbles is inhibited. During the interactions of the bubbles, the energy of each bubble, which is converted to potential energy, is less than that of single bubbles so that the bubbles cannot reach its R_0, and thus their phase is delayed. Here the
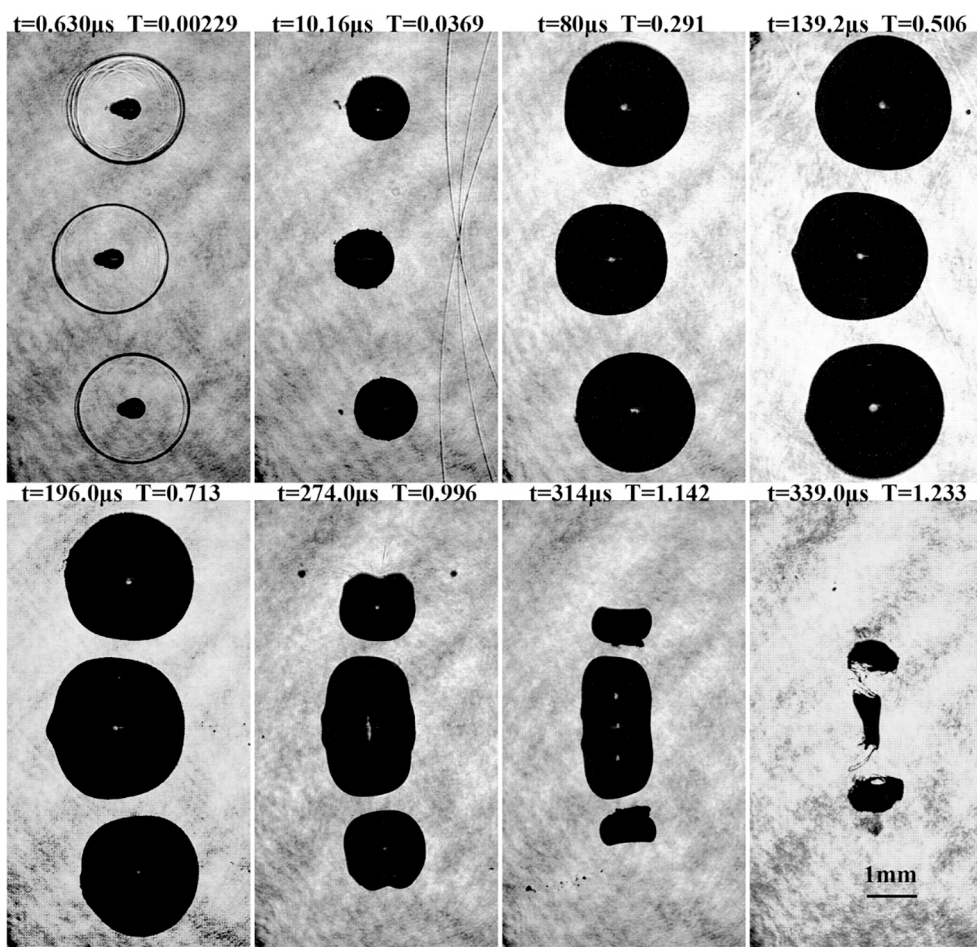
Fig. 7. Case 3: Medium γ ($\gamma = 1.0$) experimental results with intermediate interaction.
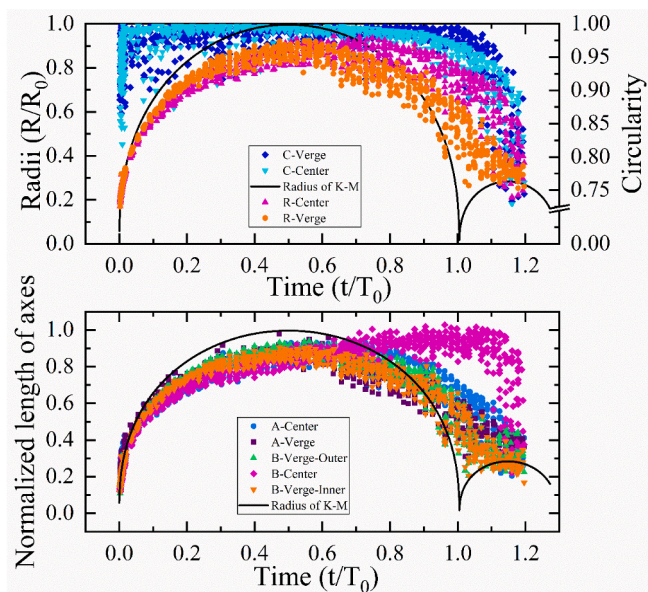

Fig. 8. Parameters in Case 3.

phase delay was followed by a decrease of maximum radii due to the limited bubble energy. The center bubble was affected by two verge bubbles simultaneously, while the two verge bubbles were only affected by the center bubble because of the screen effect [40,41]. Therefore, the center bubble is more significantly inhibited, indicating a smaller R_{max} and more phase delay than the verge bubbles. During the expansion, the A and B axes differed slightly. However, when the bubbles in both positions enter the shrinking phase, the negative radiation pressure will stretch the other bubbles, mainly on the B axis, and thereby elongating the B axis. Remarkably, the center bubble was stretched most, and hence its A and B axes were longer than that of the verge bubbles. The B-inner and B-outer based on the minimum bounding rectangle cannot accurately describe the deformation of the verge bubbles due to the concave deformation. From the image of C, the C of verge bubbles become smaller at the end of the shrinkage, that is, at $T = 1.05$. On the other hand, the center bubble loses its C at $T = 0.8$ due to the stretching. Conclusively, the motion of bubbles in Case 1 is similar to that of an isolated single bubble, but the phase is slightly prolonged, the maximum radii are slightly smaller, and deformation occurs before the collapse.

Figs. 5 and 6 present the results of Case 2, $\gamma = 1.47$. Overall, the result was similar to that of Case 1. However, the smaller spacing between the bubbles enhanced their interaction, while some effects might be more pronounced for the multi-bubble system. The initial phase exhibited very little impact, like the second frame. The phase delay was more pronounced than Case 1. In addition, the inhibition of phase due to the interaction was similar to that of Case1. Comparing the four frames of third and fourth in the bottom columns of Figs. 3 and 5, the collapse time of the two kinds of bubbles in Case 2 was delayed, with a higher time difference between the center and verge bubbles. The phase delay of the center bubble was apparent due to the dual inhibition of two verge bubbles. Thus, the T of stretching and collapse was delayed.

From the Rs graph, the curves of Case 2 are broader and lower than that of Case 1. The rebound of Case 2 is at T greater than 1.1, while that
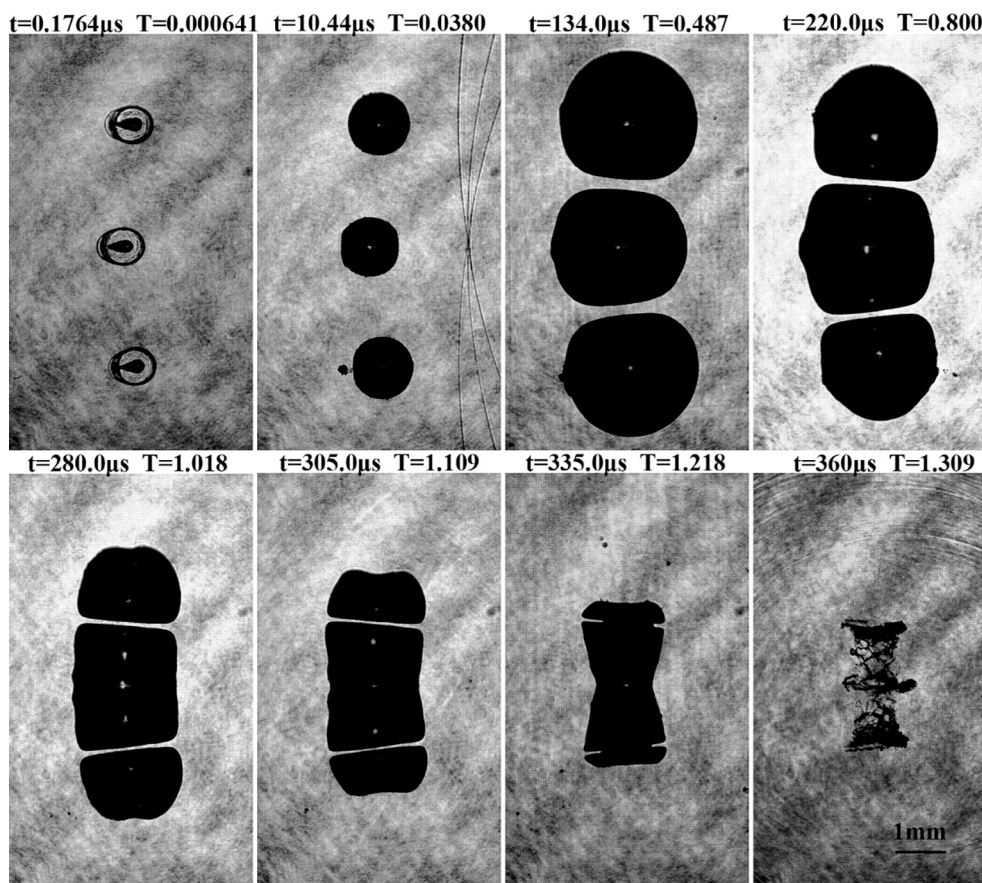
t=0.1764μs T=0.000641   t=10.44μs T=0.0380   t=134.0μs T=0.487   t=220.0μs T=0.800

t=280.0μs T=1.018   t=305.0μs T=1.109   t=335.0μs T=1.218   t=360μs T=1.309

1mm

Fig. 9. Case 4: Little γ ($\gamma = 0.80$) experimental results with the second strongest interaction.
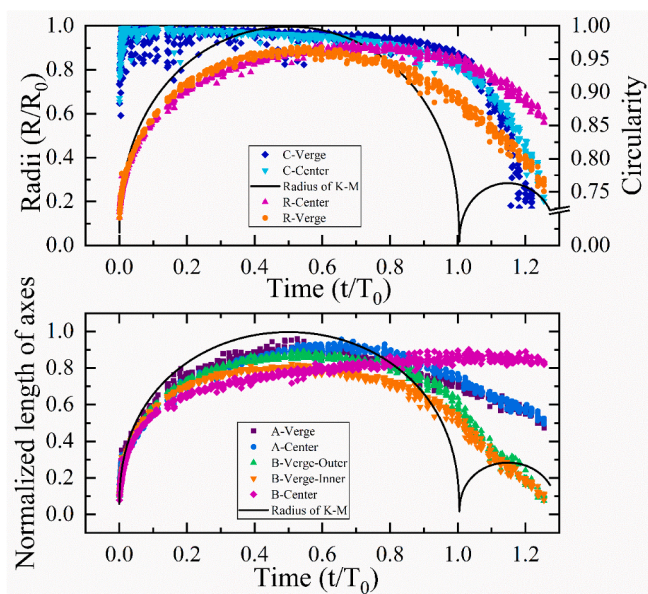

Fig. 10. Parameters in Case 4.

of Case 1 is at $T \approx 1.1$. Additionally, the maximum value of R in Case 2 was slightly lower than that of Case 1, and the reaching time is also delayed, which is the phase delay caused by inhibition. The difference between center and verge Rs also expands. From the axes graph, A, B, and R of verge bubbles are synchronized to reach the maximum and then contract, reach the minimum, and then rebound. On the other hand, A

and B of the center bubble is synchronized with R during the expansion phase and is smaller than the A and B of verge bubbles. Thus, A-center is flatter and broader than axes of verge bubbles. The B-center separates from the other axis curves at $T = 0.65$ and remains continuously high until it decreases after $T = 1.0$. This signifies the center bubble of Case 2 is elongated in the vertical direction.

Compared to Case 1, the bubble deformation in Case 2 was more pronounced. The C of verge bubbles rapidly decrease in the late stage of shrinkage, $T = 1.0$, due to the jets penetrating the bubbles. The rebound period also maintains a smaller C due to multi-bubble disturbance and unstable processes. The C of the elongated center bubble starts to decline slowly at $T = 0.65$, and eventually decreases sharply during the collapse phase. Finally, compared with Case 1, the overall deformation is more prominent, and the deformation time T is also advanced.

Figs. 7 and 8 show the results of Case 3, $\gamma = 1.0$. The interactions were more evident due to a closer spacing. As shown in the third frame of Fig. 7, the expansion of the center bubble is inhibited. Consequently, the inner edges of the verge bubbles get flattened. Therefore, the centroids of verge bubbles form an offset due to the interaction of push. The fourth frame revealed that the verge bubbles reach near their maximum radii, while the phase of the center bubble lags far behind, and also its radius does not reach the maximum. Furthermore, both kinds of bubbles deform significantly, whereas the opposite surfaces get more flattened. As a result, the centroids of verge bubbles move towards the center bubble due to the shape change. As indicated in the fifth frame, when the center bubble reaches near the maximum radius, the verge bubbles begin to shrink. Between the fourth and fifth frames, there is no contact between the three bubbles, and there exist two thick gaps of water layers, the length of which are in the range of $0.3R_0 - 0.4R_0$. Consequently, the verge bubbles shrink and form a stretch against the center bubble, as depicted in frame 6. Moreover, the verge bubbles form jets
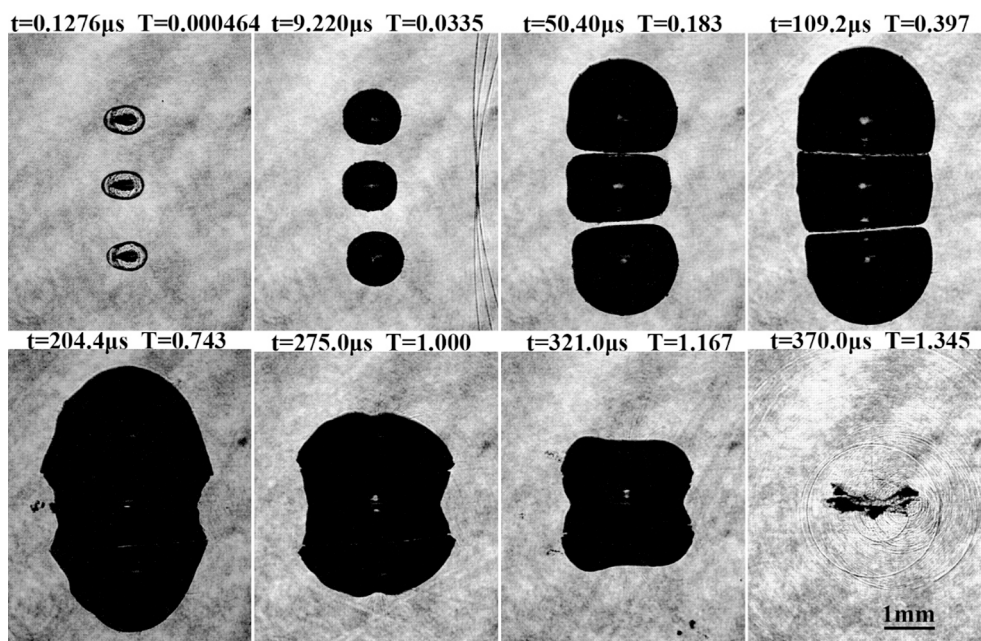
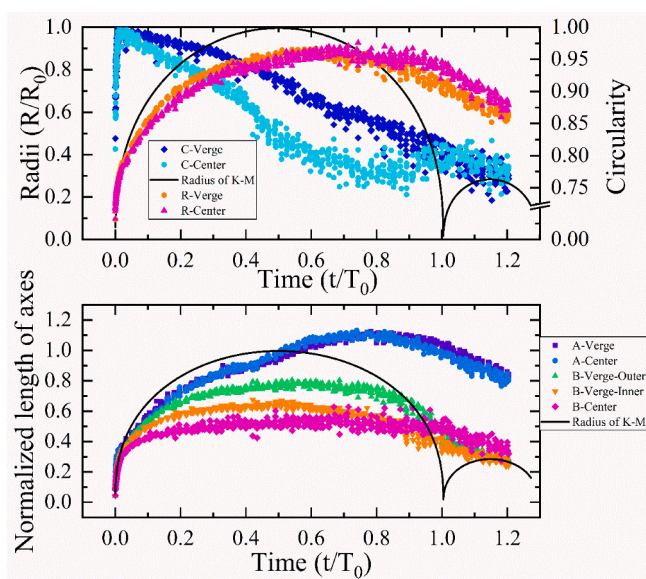**Fig. 11.** Case 5: Little γ ($\gamma = 0.45$) experimental results with the strongest interaction.

Fig. 12. Parameters in Case 5.

Fig. 13. The normalized distance of different case. Little γ receives a greater push effect.

from the outer boundary towards the center bubble. The phase difference between bubbles gradually accumulates under the influence of the interaction. The center bubble continues to grow in the vertical direction, while the horizontal shrinkage is approximately synchronized with the verge bubbles, as viewed in frames 6, 7. Lastly, the jets penetrate the verge bubbles vertically. Then the verge bubbles collapse and rebound while the center bubble collapses and rebounds horizontally (as shown in frame 8). The collapse times are delayed compared to that of Case 2.

Fig. 8 shows the normalized radii, axes, and circularity over time of Case 3. The initial expansion of bubbles follows the K-M model. When the pressure waves induced by expansion start to affect each other, the expansion is slowed down by a decrease in the differential pressure between inside and outside. As indicated in the radii graph, the R curves were clearly no longer symmetric curves of $T = T_x$ (in K-M, $T_x = 0.5$). They become smoother with the growth of span. The maximum bubble radii that can be reached by the inner and outer bubbles are larger than
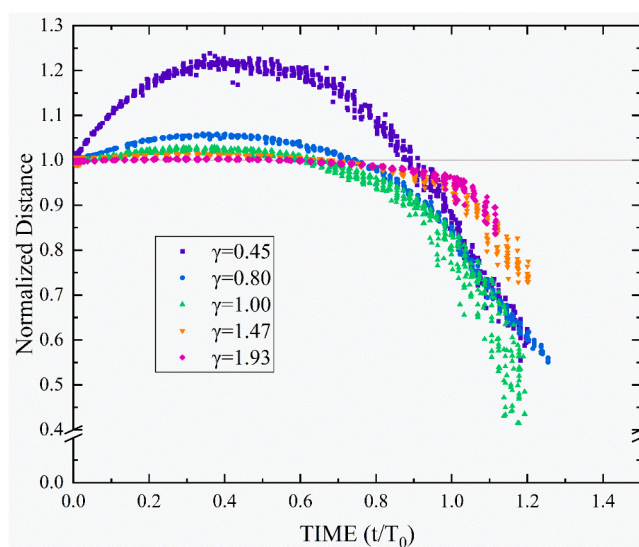
that of K-M. The verge bubbles reached their maximum R at $T = 0.5$, while the center bubble reached its maximum R at $T = 0.6$. Both the center and verge bubbles maintained stable and maximum for a longer time duration significantly. This corresponds to the interaction of the tension waves generated by the shrinkage.

Overall, the axes of verge bubbles changed similarly to R. This is also consistent with the higher C, which means the bubbles have better circularity. The A and B of the center bubble were smaller than those of verge bubbles in the expanding stage. However, the center bubble begins to change apparently at $T = 0.6$ when it reached the maximum radius. The deceleration of A-center was slower, and its height was higher than the axes of verge bubbles because there are no adhesions, and also the effect of the tension wave is greater. The B-center continues to increase linearly to approximately $T = 1.1$ and then plummets due to the occurrence of collapse. This turn occurs faster and later than that of Case 2. The B-verge -outer is higher than the B-verge-inner, which

indicates that the centroids of verge bubbles move towards the center, and their parts closer to the center bubble are wider. Finally, the deformation of the center bubble, which the A and B show, represent in C as a gradual smooth reduction starting at $T = 0.6$ and reaching a minimum at collapse.

Fig. 9and 10 show the results of Case4, $\gamma = 0.8$. From the second frame of the upper column, the initial evolution of the bubbles was still spherical. The phases of bubbles become different after the bubbles are affected by the pressure wave induced by other bubbles. In frame 3, the verge bubbles are significantly larger than the center bubble. This may be attributed to the effect of the inhibition described above. Thus the center and verge bubbles form a more evident phase difference. Whilst, the bubble expansions are inhibited, the contacted parts get flattened, and bubbles push each other. In frame 4, the verge bubbles begin to shrink. Under the combination of hydrostatic pressure, tensile force, and internal bubble pressure, the center bubble maintains maximum for a longer time than in K-M. Because of this mutual stretching, the space between the bubbles is reduced. In the frames of the bottom column, the center bubbles shrink but are also stretched by the verge bubbles to form a distinctive cylinder structure. Consequently, the opposite surfaces get flattened, while the vertical sides deform from the horizontal symmetry axis as well as the middle position of the vertical sides. In the second frame of the bottom column, distinct water films form between the bubbles. The verge bubbles collapse inward partly due to the jets. The horizontal shrinkage of the center bubbles was substantial. The opposite sides of the verge bubbles to the center bubble are stretched by the center bubble. The closer to the vertical symmetry axis and the center bubble, the slower the phase is. This phase delay creates inward jets on the outer boundaries. In frame 3 of the lower column, the jets from the verge bubble penetrates their bubbles and shoot into the center bubble, which continues to shrink, necking to a remarkable hourglass. In the later stage, the center bubble may collapse at the waist of the hourglass. In frame 4 below, the verge bubble collapses completely, and their residual gas is mixed with the residual gas from the center bubble. The phase of the center part of the center bubble is more advanced, resulting in rebound earlier than the other part. However, due to the unstable of residual gas and water, the center bubble collapses to a complex state. The time of jets forming and collapse was delayed compared to that of Case 3. In cases where γ is small enough, bubbles may develop an outspread adhesion in the opposite centers during oscillation. Although significant boundary gaps can still be observed, as disclosed in frame 7. Under this circumstance, when we processed the images, we connected the closest two points of two gaps, and deemed the lines as the boundaries of bubbles, without considering the influence of jets on R in the three-dimensional scale. Then we calculate the parameters of bubbles as mentioned in the experimental setup.

Fig. 10 outlines the normalized radii, axes, and circularity over time of Case 4. The R curves were smoother with the loss of symmetry. After reaching their maximum value, Rs changed slowly and remain at a relatively high level. The initial stage of expansion was slightly different than that of K-M. As the pressure waves from the other bubbles reached the exact bubble, its expansion was gradually inhibited. The center bubble was affected by double interactions, and thus its inhibition was bigger, which leads to its more phase delay. Additionally, the R of the center bubble was smaller than that of verge bubbles in the expansion, but bigger in shrinkage. The verge bubbles reached their maximum radii within a short time after $T = 0.5$ and then declined slowly. On the other hand, the center bubble reached its maximum radius near $T = 0.8$, and then decline slower than the verge bubbles. Here, the difference between Rs and K-M was bigger than in Case 3.

The B of the center bubble in the axes graph of Fig. 8 reveals a sharp contraction at the end of shrinkage. However, in Fig. 10, it has only two stages namely growth and stabilization. The stable stage extends to the right of the figure until the cavitation bubble is broken. Thus we can treat it as the turn we mentioned in Case 2 and 3, of this curve moved towards a positive direction. This is because after the bubble is pulled

into a cylinder, its shrinkage is mainly reflected as an hourglass shrinkage, and in deformation. After fracturing at the waist, the minimum bounding rectangle of the remnant center bubble changed slightly. The B-inner of the verge bubbles was more affected, and therefore smaller than the B-outer. In comparison, the difference between B-verge-inner and B-verge-outer become bigger than that of Case 3. This suggests that the centroid translation caused by the deformation gets more evident. The As of the center and verge bubbles change synchronously because the tension at the opposite and contact surfaces is balanced. The contraction did not occur at the width of the minimum bounding rectangle, and thus As may exhibit high value and decline slowly. The C of Case 4 starts to decline slowly at $T = 0.2$, while in Case 3 it is at $T = 0.6$. This was caused by the squeeze. Cs remain high during the expansion period. The C-center was smaller because the center bubbles are squeezed greater. When shrink, the shape of the verge bubbles is flattened by the jets, and the center bubble necks to an hourglass. Their Cs gradually get smaller and decrease violently as the shrinkage progresses. Meanwhile, the verge bubbles deform violently, resulting in a smaller C-verge.

Figs. 11 and 12 show Case 5, $\gamma = 0.45$. The second and third frames on the top column are the early stage of bubble expansion. Bubbles got flat at the opposite position to each other while the other positions expand as normal. The opposite surfaces got nearly parallel. The closer to the vertical symmetric axis, the earlier the surface becomes flat. The length of parallel surfaces increases over time before reaching the maximum. In the fourth frame on the top column, the center bubble grows to a cylinder because of the squeezing of two verge bubbles; the verge bubbles grew like straight mouth bowls with a round bottom at the same time. Water films persisted between the bubbles.

The contact surfaces continue expanding due to the increased pressure difference caused by the bubble interaction. The verge bubbles evolved into an open bowl, while the side of the center bubble looks like a hyperbola. The central part of the center bubble started to shrink as the internal pressure was released. The squeezing caused the parts to move out of phase, and the bubbles were unable to reach their maximum radii at the same time. In the vertical parts of the bubbles, the phase was more advanced, whereas, in the second frame in the lower column, the upper and lower bubbles form jets in the vertical symmetrical axis. Additionally, we can still observe the delineation of bubbles. Since the phase at the contact parts was delayed, the bubbles as a whole exhibited a cross shape shrinkage. The phase of the non-contact parts of the center bubble was later than that of the verge bubbles due to the double action of the other two bubbles. The cross shrinkage is mainly reflected in the vertical direction. The last frame indicated that the bubbles finally collapse vertically and radiate shockwaves outwards, ending up a dish-shaped remnant. The center bubble was smaller than the verge bubbles in the expansion but bigger in the shrinkage. Overall, the lifetimes of the three bubbles were nearly equal, and being longer than those in Case 4.

Fig. 12 shows the normalized radii, axes, and circularity over the normalized time of Case 5. The Rs still obeyed the K-M model of isolated single bubble expansion in the early stage of cavitation. When the pressure fields of bubbles induced begin to influence each other, the pressure waves increase the external pressure and hence reduced the pressure difference. Thus, the progress of R was inhibited. The asymmetry of R curves gets more evident. When expanded, the center bubble was subjected to the pressure wave of both verge bubbles. Its external pressure is higher than the others, the pressure difference is less, and the inhibition is larger, while the verge bubbles are only affected by the pressure of the center bubble due to the isolation effect of the center bubble, and also receive less inhibition. Therefore, the verge bubbles reach the maximum radii before the center bubble, but later than that of an isolated single bubble in the first oscillation period. The difference between maximum Rs of the center bubble and that of the verge bubbles reached was small. Besides, they are all smaller than those in the K-M model and Case 4. Meanwhile, Rs changes more slightly than in Case 4. In the early shrink stage, the internal pressure was lower than the

external pressure. Bubbles radiate a pulling force pointing to itself. Therefore, the difference between the internal and external pressure of other bubbles become less, and the oscillation gets inhibition. Bubbles shrink synchronously in the vertical; thus, the difference between Rs of the center and verge bubbles are small. Generally, for the center bubble, the period was more extensive; the phase was delayed due to it receiving larger inhibition.

On the axes graph, we can observe the inhibitory effect more clearly. At the primary stage of the bubble, it expands rapidly. After the normalized length reaches about 0.3, the expansion slowed down significantly. Then Bs stabilizes near the maximum and slowly declines after reaching the maximum. The B-inners were more severely affected, which represents the length of the opposite surface to the centroids. When B-verge-inner + B-center = 0.9 = 2*γ, the edges of the isolated expanding bubbles should contact each other. However, we observed in the column above, that there was a presence of water film. The continuous growth of the short axis was accompanied by the displacement of the relative position of bubbles. The interaction between the bubbles forms a push that pushes the verge bubbles away from the center bubbles. As mentioned above, the center bubble is affected by two pressure fields, while the verge bubbles were affected by only one pressure field. Thus, B of the center bubble is smaller than that of the verge bubbles. In addition, the difference between B-verge-outer and B-verge-inner was more apparent than that of Case 4. This purports that the shift of verge bubble centroids is considerable while the mutual extension of the inter-bubble joints is stable (Table 1).

Particularly, when $T = 0.4$, the Bs reach the maximum, as well the bubble distances, as denoted in Fig. 11, upper frame 4. After this point, the bubble energy is released mainly through the mutual extension of the inter-bubble joints. Subsequently, As refers to the length of the joint, which appears a process of re-growth. In this re-growth progress, the As of center and verge bubbles change synchronously and reach their maximum at approximately $T = 0.8$. However, there exists a small difference because the center bubble shrinks horizontally while the verge bubbles predominantly shrink along the vertical direction. Hence, the axes cannot accurately describe the bowl-shaped deformation of verge bubbles and the hyperbolic deformation of the center bubble. Therefore, C becomes an excellent auxiliary parameter to describe the deformation. From the circularity graph in the upper column of Fig. 12, it can be viewed that the beginning of the circularity loss is earlier than $T = 0.1$. The deformation of the center bubble is more than that of verge bubbles. Then at $T = 0.4$, the C-center dropped a sudden. This progress corresponds to the mutual extension of the inter-bubble joints after the bubbles contact each other. The C flatten out when the R reaches the maximum, and rise due to the global shrinkage of the center bubble. Afterward, it declined after $T = 1.0$ because the vertical shrinkage of the center plays a significant role.

Fig. 13 shows the results of normalized bubble distance, $\tilde{D}$ over time in case 5. $\tilde{D}$ can be used as a measure of the bubble interactions, while $\tilde{D} = 1$ represents the initial position of the bubble center. A bigger $\tilde{D}$ indicates that the bubbles are far away from each other, whereas a smaller $\tilde{D}$ means they are close to each other. Furthermore, $\tilde{D}$ reflects the effect of bubbles radiated pressure waves on other bubbles. Also, it shows the movement of verge bubbles, while on the other hand, it reflects their deformation. If the proximal and distal ends are fixed, the deformation also changes the centroids. The flattening of the opposite surface of bubbles makes $\tilde{D}$ smaller. Likewise, jets produced and penetrated

inwards would also make $\tilde{D}$ smaller. Here, the effects of these two factors are considered indiscriminately as the centroid distance change is caused by bubbles interaction.

Due to the geometrical attenuation of the radiated pressure waves, the closer the position is in the same direction of the assumed spherical bubble, the stronger is the sound pressure. The smaller the γ is, the larger the ratio of stress surface to radiation wave sphere is, and the more evident is the forced effect. Therefore, the smaller the γ is, the more apparent is the effect of the inter-bubble force. As shown in the graph, the smaller the γ is, then, the larger the maximum value of $\tilde{D}$ is, the faster the $\tilde{D}$ changes, and the later $\tilde{D}$ reaches its maximum. This indicates that the closer the bubbles are to each other, the more energy is used to push the adjacent bubbles away. After $\tilde{D}$ exceeds 1, the time of falling below 1 decreases with γ increasing. This means the bigger the γ is, the sooner it can stop pushing each other around and return to its original position. In the shrinking phase before $T = 1.0$, that is, none bubbles have rebounded, the smaller the γ is, the steeper the curve becomes. Thus it indicates that the larger the γ is, the greater the potential energy accumulated, the longer the acceleration distance is, and the faster the movement is. These also tell that the time duration of the negative pressure radiated by bubbles is broad enough to complete the process.

When $\gamma = 1.93$, the push between the bubbles is almost negligible. However, in the shrinking phase, $\tilde{D}$ decreases, in part due to the proximity of bubbles, as well as the deformation caused by jets. In the rebound phase, the verge bubbles penetrated by jets rebound with movement inward, thus the $\tilde{D}$ decreases.

In Case 2, $\gamma = 1.47$, it can be noted that the part above $\tilde{D} = 1$ has a certain curvature. The push effect was greater than Case 1. Meanwhile, at the pull stage, the curve turns earlier.

When $\gamma = 1.0$, the push and pull between bubbles were notable. The difference in the time phase between bubbles increases, while the center bubble collapses laterally in a stick shape with stable length. Moreover, the verge bubbles re-expanded in the direction of the jets, $\tilde{D}$ decreases significantly.

In the case of $\gamma = 0.8, 0.45$, the push and pull between bubbles were more apparent. At the shrinking phase of Case 4, the center bubble collapsed in an hourglass shape. Also, it may disintegrate at the vertical center. Thereafter, the two separated parts will move outward and merge with verge bubbles, and then collapse near the position of verge bubbles. Therefore, in this case, the $\tilde{D}$ is small but larger compared to that in case 3. On the other hand, in Case 5, center and verge bubbles collapsed in a disk-shape. The denominator of $\tilde{D}$, D_0, is little enough so that the change in the trend of $\tilde{D}$ is not too obvious. Besides, the phase difference between center and verge bubbles was quite little at collapse, so that simultaneous collapse and rebounding does not occur.

4. Discussion

Bubbles can be treated as symmetrically aligned in-phase bubbles, taking into account the isolation effect and ignoring the small angular shifts in the arrangement between the bubbles. The behavior of bubbles at different positions can be approximated to different existing examples. For instance, the center bubble is restricted in two directions, and its oscillation is similar to that of a bubble between two parallel rigid boundaries. The verge bubbles, on the other hand, are inhibited in one direction and thus exhibit similar patterns as if they were bubbles near a rigid boundary. Jets are formed towards the center bubble during the shrinking phase. However, in the experiments, since the three laser beams are focused from the same lens, there is an inevitable focus shift at a larger incident angle at the time of breakdown. Thus the three points are not strictly linearly aligned but form a specific small angular offset. At this point, the interactions between the bubbles are different from the aforementioned analogy. The center bubble receives the action of bubbles on both sides, not in a straight line, but an angle. The behavior of

Table 1
Normalized bubble energy $\tilde{E}$

	$\gamma = 0.45$	$\gamma = 0.80$	$\gamma = 1.0$	$\gamma = 1.47$	$\gamma = 1.93$
Center bubble	0.7360	0.7584	0.7895	0.7833	0.8507
Verge bubbles	0.7115	0.7216	0.7502	0.7994	0.8702
Sum	2.1590	2.2015	2.2898	2.3820	2.5911

center bubbles can be analogized to bubbles in different angular structures. In the experimental figures, the left and right boundaries of the center bubbles during the shrinking phase are not symmetrical. Notably, in Figs. 9 and 11, the shape of the formed jets are asymmetric. These are all problems caused by the directionality of multiple pressures. The situation can be approximated as described elsewhere [52–57] partly. Here, we ignore the little angular shift due to the screen effect and symmetry. The interaction between the bubbles can be simplified as the interaction between bubbles and their acoustic radiation When the bubble is a spherical one, the time-varying sound pressure of its far-field can be expressed as follows:

$$p_a(r, t) = \frac{\rho_L}{4\pi r} \frac{d^2 V}{dt^2}, \tag{1.6}$$

where p_a refers to the sound pressure of the far-field radiation, r refers to the distance from the center of the bubble to the measuring point, ρ_L refers to the liquid density, and $V(t)$ represents the time-varying volume of the bubble [49]. After determining the measuring position and the relative direction of the bubble, it is reasonable to extend this formula to the radiation acoustic pressure of non-spherical bubbles based on the change of the bubble radius in one direction [58], which is

$$p_a(R, r, t) = \frac{\rho_L}{r} \cdot R \cdot \left(2\dot{R}^2 + R\ddot{R}\right), \tag{1.7}$$

where $R(t)$ refers to the change of bubble radius along the direction of r. By substituting this sound pressure to the external acoustic pressure term $p(t)$ in the K-M model, the pulsation of the bubbles affected by the far-field sound pressure can be obtained. The dimensional situation studied in this paper cannot be completely expressed by the far-field pressure. When being affected, the bubbles will lose their sphere, while their boundary and the pressure of the outward radiation will change. However, it is still quite reasonable to explain the effects suffered by bubbles using sound pressure [41]. In this regard, we can simply divide the affected bubble radiation pressure into three processes. See attached Figure 23 from the literature [51]: *stage a.* high-pressure pulses and constantly decreased positive pressures in the initial expansion phase; *stage b.* negative pressure in the stable phase; and *stage c.* positive pressure and high-pressure pulses formed at the end of the shrinkage. As mentioned earlier, the *stage a* may slow down the expansion of bubbles. Moreover, the center bubble is affected by multiple *stage a*s and becomes slower. The *stage b* increases the expansion, blocks the shrinkage and causes the stretching of the bubbles, which maintain a large radius in the direction of the force for more time. The *stage c* accelerates the collapse or decelerate the rebound of adjacent bubbles. Since the affected collapse is directional, the results of the mentioned cases are also different. For example, in Case 1–2, the pressure of the verge bubble on the center bubble almost cancels out the deformation caused by *stage b*, while the center bubble does inhibit the rebound of the verge bubbles. In Case3 − 4, the shrinkage of the center bubble is primarily reflected in the horizontal direction. Thus, the pressure wave of center bubble formed in *stage b* and *stage c* is mainly transmitted in the horizontal direction. It is difficult to influence the verge bubbles. The effect of the verge bubbles on the center bubble is reflected in the flattening of the opposite surfaces and accelerated contraction. In Case 5, due to its proximity and phase synchronization, the three bubbles can be considered as a whole, and thus the effects of *stage c* can be ignored.

The pressure waves associated with the above three stages modify the distribution of internal and external pressure of adjacent bubbles, instead of uniform pressure difference as isolated spherical bubbles. The internal and external pressure distribution of the bubbles is determined by direction, which makes the oscillation of the bubbles in different directions show a large difference. Thus, we can assume that the radius change in different directions within a bubble has different periods, that is, a bubble has different time phases in different directions. In a bubble,

the phase is delayed, where it is affected by pressure waves. For instance, where the external pressure is higher, the phase is highly delayed. The direction with the later phase reaches the maximum radius later as well as the minimum radius, namely collapse. As a result, deformation will occur. The part with the advance phase reaches the maximum, while the other one with the later phase does not reach the maximum. Then the advance phase part begins to shrink, whereas the part with the later phase has just reached its maximum. This process is often accompanied by the transposition of the bubble long axis. When the advance phase part starts to shrink sharply, the delayed phase part just starts to shrink. Therefore, forming specific deformation, for example, jets from the advance phase part to the delayed part.

In this work, the center bubble experienced more pressure than the verge bubbles. In addition, the ensemble phase of the center bubble was delayed more compared to that of verge bubbles. Hence, the lifetime of a center bubble is longer, the radius smaller than verge bubbles. When one specifically analyzes the individual bubble, the center bubble is first affected by the pressure wave along the vertical direction. Thus the phase delay decreases as the distance from the opposite surface to a certain position vertically increases. The central part is affected later; the phase is in advance. Therefore, as described earlier, the axis transposition, special cylindrical shape, and special forms of collapse will form. Moreover, the opposite position of the verge bubbles to the center bubble is first affected by the pressure wave, and thus its phase is later. On the other hand, the backside position in the verge bubbles is later affected by the pressure wave, and thus the phase is in advance. As a result, the oscillation of the leeward boundary in the verge bubbles precedes the windward boundary. The leeward boundary shrinks violently while the windward boundary is in the stable stage. Then the inward jet is formed on the leeward boundary. The verge bubbles in different cases form jets at different times, due to their different time phase difference between their anterior and posterior surfaces.

This method of dividing the interior of bubbles into different phases can be extended to the bubble arrays. Each bubble in the array can be treated as a part of the bubble described above. As noted in the literature [59], since the corner bubbles are further away from the geometric center, it can be treated as the expanded parts with advanced phase in a single bubble by analogy. Hence collapse starts from an angle rather than the edge. This perhaps may be another way to understand the direction of the collapse except for curvature.

Geometrically, for the R, we define based on shadow, and for a volume given bubble, the spherical bubble has the smallest max(R). Furthermore, the max(R) might become larger when bubbles lose their sphericity in deformation. In the interaction of the multiple bubbles, if the volume of the bubble does not change, the max(R) should be larger. However, each of the max(R) we measured was becoming smaller, which suggests that the volume of the bubbles affected by the interaction did not reach the maximum volume that the isolated bubbles can reach.

The process of bubble expansion can be regarded as a process of kinetic energy transformed into potential energy. When the internal pressure of a bubble is greater than the external pressure, it is therefore the difference between the internal and external pressure that drives work to achieve the transformation. After exceeding the equilibrium radius, the internal pressure of the bubble is less than the external pressure. The bubble transforms the residual kinetic energy into potential energy through inertia. When multiple bubbles interact, the bubble energy is not only transformed from kinetic energy to potential energy but also a part of the kinetic energy transfer that makes the bubble position move relatively. During expansion, there is a push effect in bubbles that keeps adjacent bubbles away from themselves. When bubbles are far away, the multi-bubble system accumulates potential energy. During shrinkage, the potential energy of the bubble system is transformed into kinetic energy, including the kinetic energy of bubble shrinkage as well as the bubble movement. This process is a unified process relevant to the equilibrium radius. However, since the driving

force of the two transformations in this process is not the same one, they have some independence. Thus, the time of the maximum bubble radius and the maximum distance do not coincide.

Without the consideration of the change of deformation to R, $\max(R)$ is directly used to calculate the bubble energy $E = (4/3)\pi(\max(R))^3 p_0$. The normalized bubble energy $\tilde{E}$ is obtained by comparing it to E_0, using R_0 in the energy equation.

In the table above, the maximum 20 values for each set of R are averaged and then calculate $\tilde{E}$. The Sum column is the result of one center bubble plus two verge bubbles. It can be noted that as γ decreases, the bubble energy contained in bubbles with maximum radius is declining. This implies that the bubble energy transformed into the bubble potential energy is increasing, which is consistent with our results of the pushing distance $\tilde{D}$.

5. Conclusion

In this work, the dynamics of three uniformly separated laser-induced bubbles were experimentally studied. The precise control of distance and energy achieves the multi-bubbles interaction in one life period under ideal conditions. As a parameter of evenly distributed multi-cavitation space, γ is the main parameter in this study. The study shows:

1. In bubble arrays, the lifetime of each bubble is generally extended, while the volume is reduced. This phenomenon is most apparent for the center bubble because of the most inhibition it received. In shrinkage, the lifetime difference causes the collapse of bubbles to proceed in an orderly manner, from the outside to the inside. Meanwhile, the smaller the γ, the more evident is this phenomenon.
2. The different phase delay in different parts of a bubble causes the unique shape of bubbles. From a relatively independent perspective, it can be considered that for the inner part of a bubble, the closer it is to the adjacent bubble, the more the phase delay. This phenomenon is achieved through the interaction between the bubbles and the acoustic radiation of the cavitation pulsation. The acoustic radiation changes the pressure difference between the interior and exterior of bubbles, which has an inhibitory effect on the continuous motion at the corresponding pulsation phase, thus delaying the phase of bubble parts.
3. In the three-bubble system with the same initial phase and equal spacing, there are various forms of the collapse of the center bubble: normal collapse; slightly elongated in the direction of alignment; elongating to a long stick; necking to an hourglass. When the γ is sufficiently small, the compression effect is more efficacious than stretching, then the center bubble was compacted to a dish. The center bubbles do not produce jets, while the verge bubbles produce jets towards the center, and the jets become stronger as the γ decreases. The beginning of the loss of circularity, which generally indicates the stability of the shape of bubbles, can occur at any stage. It moves forward as the γ decreases, from the end of shrinkage to the beginning of bubbles.
4. During the oscillation of the bubble array, the bubbles interact with each other through acoustic radiation, and the energy transfer changes the relative position of the bubbles. In expansion, the verge bubbles are pushed outward, while in shrinkage, they are pulled inward. The smaller the γ, the more apparent is the phenomenon.

The interaction of multiple cavitation bubbles is discussed in this paper. The parameters R, A, B, C, and D are used to describe the interaction. However, further parameters describing the deformation during the interaction are needed especially in future research. Also, the lifetime extensions require to be quantified. The fate of the cavitation energy needs more accurate measurements. Whilst, the experimental method should be improved to obtain more accurate information about

the bubbles in interaction. Therefore, further improvement should focus on the multiple bubbles dynamics in more detailed cases of parameter $\gamma < 1$. Of note, this research provides valuable information for further understanding of the mechanism of multiple cavitation bubbles in medical and hydraulic engineering.

CRediT authorship contribution statement

Hengzhu Bao: Conceptualization, Validation, Investigation, Software, Visualization, Writing - original draft, Writing - review & editing. **Hongchao Zhang:** Methodology, Resources. **Lou Gao:** Investigation. **Mao Tang:** Software, Validation. **Chong Zhang:** Writing - review & editing. **Jian Lu:** Supervision, Funding acquisition.

Declaration of Competing Interest

The authors declare that they have no known competing financial interests or personal relationships that could have appeared to influence the work reported in this paper.

Acknowledgments

References

[1] N. Ochiai, J. Ishimoto, Numerical analysis of the effect of bubble distribution on multiple-bubble behavior, Ultrason. Sonochem. 61 (2020), 104818, https://doi.org/10.1016/j.ultsonch.2019.104818.

[2] R. Timm, Optical and acoustic investigations of the dynamics of laser-produced cavitation bubbles near a solid boundary, J. Fluid Mech. 206 (1989) 299–338, https://doi.org/10.1017/S0022112089002314.

[3] S. Li, Cavitation enhancement of silt erosion—an envisaged micro model, Wear 260 (2006) 1145–1150, https://doi.org/10.1016/J.WEAR.2005.07.002.

[4] W. Lauterborn, H. Bolle, Experimental investigations of cavitation-bubble collapse in the neighbourhood of a solid boundary, J. Fluid Mech. 72 (1975) 391–399, https://doi.org/10.1017/S0022112075003448.

[5] P. Cui, A.-M.-M. Zhang, S. Wang, B.C. Khoo, Ice breaking by a collapsing bubble, J. Fluid Mech. 841 (2018) 287–309, https://doi.org/10.1017/jfm.2018.63.

[6] N. Vyas, Q.X. Wang, K.A. Manmi, R.L. Sammons, S.A. Kuehne, A.D. Walmsley, How does ultrasonic cavitation remove dental bacterial biofilm? Ultrason. Sonochem. 67 (2020), 105112 https://doi.org/10.1016/j.ultsonch.2020.105112.

[7] C. Ohl, T. Kurz, R. Geisler, O. Lindau, W. Lauterborn, Bubble dynamics, shock waves and sonoluminescence, Philos. Trans. R. Soc. London. Ser. A Math. Phys. Eng. Sci. 357 (1999) 269–294, https://doi.org/10.1098/rsta.1999.0327.

[8] P.M. Kanthale, P.R. Gogate, A.B. Pandit, A. Marie Wilhelm, Cavity cluster approach for quantification of cavitational intensity in sonochemical reactors, Ultrason. Sonochem. 10 (2003) 181–189, https://doi.org/10.1016/S1350-4177(03)00088-9.

[9] F. Reuter, S. Lesnik, K. Ayaz-Bustami, G. Brenner, R. Mettin, Bubble size measurements in different acoustic cavitation structures: Filaments, clusters, and the acoustically cavitated jet, Ultrason. Sonochem. 55 (2019) 383–394, https://doi.org/10.1016/j.ultsonch.2018.05.003.

[10] D.H. Peregrine, The Acoustic Bubble. By T. G. Leighton. Academic Press, 1994. 613 pp. 95. ISBN 0-12-441920-8. J. Fluid Mech. 272 (1994) 407–408. https://doi.org/10.1017/S0022112094214519.

[11] V.I.I.I. Lord Rayleigh, On the pressure developed in a liquid during the collapse of a spherical cavity, London, Edinburgh, Dublin Philos. Mag. J. Sci. 34 (1917) 94–98, https://doi.org/10.1080/14786440808635681.

[12] W. Lauterborn, C.D. Ohl, Cavitation bubble dynamics, Ultrason. Sonochem. (1997), https://doi.org/10.1016/S1350-4177(97)00009-6.

[13] M. Reiner, On volume-or isotropic flow as exemplified in the creep of concrete, Flow Turbul. Combust. 1 (1949) 475.

[14] E.A. Brujan, K. Nahen, P. Schmidt, A. Vogel, Dynamics of laser-induced cavitation bubbles near an elastic boundary, J. Fluid Mech. 433 (2001) 251–281, https://doi.org/10.1017/S0022112000003347.

[15] D. Obreschkow, P. Kobel, N. Dorsaz, A. De Bosset, C. Nicollier, M. Farhat, Cavitation bubble dynamics inside liquid drops in microgravity, Phys. Rev. Lett. (2006), https://doi.org/10.1103/PhysRevLett.97.094502.

[16] S. Poulain, G. Guenoun, S. Gart, W. Crowe, S. Jung, Particle motion induced by bubble cavitation, Phys. Rev. Lett. 114 (2015), 214501, https://doi.org/10.1103/PhysRevLett.114.214501.

[17] J.B. Keller, M. Miksis, Bubble oscillations of large amplitude, J. Acoust. Soc. Am. 68 (1980) 628–633, https://doi.org/10.1121/1.384720.

[18] W. Lauterborn, T. Kurz, Physics of bubble oscillations, Reports Prog. Phys. 73 (2010), 106501, https://doi.org/10.1088/0034-4885/73/10/106501.

[19] J.R. Blake, G.S. Keen, R.P. Tong, M. Wilson, Acoustic cavitation: the fluid dynamics of non-spherical bubbles, Philos. Trans. R. Soc. A Math. Phys. Eng. Sci. 357 (1999) 251–267, https://doi.org/10.1098/rsta.1999.0326.

[20] A. Biesheuvel, L.V. Wijngaarden, Two-phase flow equations for a dilute dispersion of gas bubbles in liquid, J. Fluid Mech. 148 (1984) 301–318, https://doi.org/10.1017/S0022112084002366.

[21] D.Z. Zhang, A. Prosperetti, Ensemble phase-averaged equations for bubbly flows, Phys. Fluids 6 (1994) 2956–2970, https://doi.org/10.1063/1.868122.

[22] D. Fuster, T. Colonius, Modelling bubble clusters in compressible liquids, J. Fluid Mech. 688 (2011) 352–389, https://doi.org/10.1017/jfm.2011.380.

[23] M. Arora, C.D. Ohl, D. Lohse, Effect of nuclei concentration on cavitation cluster dynamics, J. Acoust. Soc. Am. 121 (2007) 3432, https://doi.org/10.1121/1.2722045.

[24] G. Servant, J.L. Laborde, A. Hita, J.P. Caltagirone, A. Gérard, On the interaction between ultrasound waves and bubble clouds in mono- and dual-frequency sonoreactors, Ultrason. Sonochem. 10 (2003) 347–355, https://doi.org/10.1016/S1350-4177(03)00105-6.

[25] E. Johnsen, T. Colonius, Shock-induced collapse of a gas bubble in shockwave lithotripsy, J. Acoust. Soc. Am. 124 (2008) 2011–2020, https://doi.org/10.1121/1.2973229.

[26] M.R. Betney, B. Tully, N.A. Hawker, Y. Ventikos, Computational modelling of the interaction of shock waves with multiple gas-filled bubbles in a liquid, Phys. Fluids 27 (2015) 1–28, https://doi.org/10.1063/1.4914133.

[27] W. Lauterborn, T. Kurz, R. Geisler, D. Schanz, O. Lindau, Acoustic cavitation, bubble dynamics and sonoluminescence, Ultrason. Sonochem. 14 (2007) 484–491, https://doi.org/10.1016/j.ultsonch.2006.09.017.

[28] A. Shima, The natural frequencies of two spherical bubbles oscillating in water, J. Basic Eng. 93 (1971) 426–431, https://doi.org/10.1115/1.3425268.

[29] H.N. Oguz, A. Prosperetti, A generalization of the impulse and virial theorems with an application to bubble oscillations, J. Fluid Mech. 218 (1990) 143, https://doi.org/10.1017/S0022112090000957.

[30] R. Mettin, I. Akhatov, U. Parlitz, C.D. Ohl, W. Lauterborn, Bjerknes forces between small cavitation bubbles in a strong acoustic field, Phys. Rev. E 56 (1997) 2924–2931, https://doi.org/10.1103/PhysRevE.56.2924.

[31] A. Harkin, T.J. Kaper, A. Nadim, Coupled pulsation and translation of two gas bubbles in a liquid, J. Fluid Mech. 445 (2001) 377–411, https://doi.org/10.1017/S0022112001005857.

[32] A. Shima, T. Fujiwara, The behavior of two bubbles near a solid wall, Arch. Appl. Mech. 62 (1992) 53–61, https://doi.org/10.1007/BF00786681.

[33] B. Han, K. Köhler, K. Jungnickel, R. Mettin, A. Vogel, Dynamics of laser-induced bubble pairs, J. Fluid Mech. 771 (2015) 706–742, https://doi.org/10.1017/jfm.2015.183.

[34] S.W. Fong, D. Adhikari, E. Klaseboer, B.C. Khoo, Interactions of multiple spark-generated bubbles with phase differences, Exp. Fluids 46 (2009) 705–724, https://doi.org/10.1007/s00348-008-0603-4.

[35] P.A. Quinto-Su, C.D. Ohl, Interaction between two laser-induced cavitation bubbles in a quasi-two-dimensional geometry, J. Fluid Mech. 633 (2009) 425–435, https://doi.org/10.1017/S0022112009008064.

[36] P. Cui, Q.X. Wang, S.P. Wang, A.M. Zhang, Experimental study on interaction and coalescence of synchronized multiple bubbles, Phys. Fluids 28 (2016), https://doi.org/10.1063/1.4939007.

[37] W. Lauterborn, T. Kurz, R. Mettin, C.D. Ohl, Experimental and Theoretical Bubble Dynamics (2007), https://doi.org/10.1002/9780470141694.ch5.

[38] H. Chen, Z. Chen, Y. Li, Modulation of the secondary Bjerknes force in multi-bubble systems, Ultrason. Sonochem. 61 (2020), 104814, https://doi.org/10.1016/j.ultsonch.2019.104814.

[39] J.P. Dear, J.E. Field, A.J. Walton, Gas compression and jet formation in cavities collapsed by a shock wave, Nature 332 (1988) 505–508, https://doi.org/10.1038/332505a0.

[40] J.P. Dear, J.E. Field, A study of the collapse of arrays of cavities, J. Fluid Mech. 190 (1988) 409–425, https://doi.org/10.1017/S0022112088001387.

[41] N. Bremond, M. Arora, C.D. Ohl, D. Lohse, Interaction of cavitation bubbles on a wall, Phys. Fluids 18 (2006), 121505, https://doi.org/10.1063/1.2396922.

[42] N. Bremond, M. Arora, C.D. Ohl, D. Lohse, Controlled multibubble surface cavitation, Phys. Rev. Lett. 96 (2006) 1–4, https://doi.org/10.1103/PhysRevLett.96.224501.

[43] E. Lauer, X.Y. Hu, S. Hickel, N.A. Adams, Numerical investigation of collapsing cavity arrays, Phys. Fluids 24 (2012), https://doi.org/10.1063/1.4719142.

[44] L.W. Chew, E. Klaseboer, S.W. Ohl, B.C. Khoo, Interaction of two differently sized oscillating bubbles in a free field, Phys. Rev. E – Stat. Nonlinear, Soft Matter Phys. 84 (2011) 1–11, https://doi.org/10.1103/PhysRevE.84.066307.

[45] S. Hysing, S. Turek, D. Kuzmin, N. Parolini, E. Burman, S. Ganesan, L. Tobiska, Quantitative benchmark computations of two-dimensional bubble dynamics, Int. J. Numer. Meth. Fluids 60 (2009) 1259–1288, https://doi.org/10.1002/fld.1934.

[46] D. Kröninger, K. Köhler, T. Kurz, W. Lauterborn, Particle tracking velocimetry of the flow field around a collapsing cavitation bubble, Exp. Fluids 48 (2010) 395–408, https://doi.org/10.1007/s00348-009-0743-1.

[47] C. Zhang, J. Lu, H. Zhang, Z. Shen, X. Ni, Transient coupling model of plasma and laser field in water, IEEE J. Quantum Electron. 52 (2016), https://doi.org/10.1109/JQE.2016.2588465.

[48] W. Lauterborn, A. Vogel, Shock wave emission by laser generated bubbles, 2013. doi:10.1007/978-3-642-34297-4_3.

[49] C.E. Brennen, in: Cavitation and bubble dynamics, Cambridge University Press, 2013, https://doi.org/10.1017/CBO9781107338760.

[50] C.D. Ohl, S.W. Ohl, ShockWave interaction with single bubbles and bubble clouds, in: Bubble Dyn. Shock Waves, Springer, Berlin Heidelberg, 2013, pp. 3–31, https://doi.org/10.1007/978-3-642-34297-4_1.

[51] L. Lv, Y. Zhang, Y. Zhang, Experimental investigations of the particle motions induced by a laser-generated cavitation bubble, Ultrason. Sonochem. 56 (2019) 63–76, https://doi.org/10.1016/j.ultsonch.2019.03.019.

[52] B. Han, J. Chen, Z.H. Shen, J. Lu, X.W. Ni, Investigation of the wedge-shaped propelled surface for laser propulsion in water environment, Opt. Laser Technol. 43 (2011) 604–608, https://doi.org/10.1016/j.optlastec.2010.08.008.

[53] E.A. Brujan, H. Takahira, T. Ogasawara, Planar jets in collapsing cavitation bubbles, Exp. Therm Fluid Sci. 101 (2019) 48–61, https://doi.org/10.1016/j.expthermflusci.2018.10.007.

[54] E.A. Brujan, Y. Matsumoto, Shock wave emission from a hemispherical cloud of bubbles in non-Newtonian fluids, J. Nonnewton. Fluid Mech. 204 (2014) 32–37, https://doi.org/10.1016/j.jnnfm.2013.12.003.

[55] Y. Tomita, P.B. Robinson, R.P. Tong, J.R. Blake, Growth and collapse of cavitation bubbles near a curved rigid boundary, J. Fluid Mech. 466 (2002) 259–283, https://doi.org/10.1017/S0022112002001209.

[56] F.I. Azam, B. Karri, S.-W. Ohl, E. Klaseboer, B.C. Khoo, Dynamics of an oscillating bubble in a narrow gap, Phys. Rev. E 88 (2013), 043006, https://doi.org/10.1103/PhysRevE.88.043006.

[57] P.A. Quinto-Su, K.Y. Lim, C.D. Ohl, Cavitation bubble dynamics in microfluidic gaps of variable height, Phys. Rev. E – Stat. Nonlinear, Soft Matter Phys. 80 (2009), 047301, https://doi.org/10.1103/PhysRevE.80.047301.

[58] Y. Zhang, Y. Zhang, S. Li, The secondary Bjerknes force between two gas bubbles under dual-frequency acoustic excitation, Ultrason. Sonochem. 29 (2016) 129–145, https://doi.org/10.1016/j.ultsonch.2015.08.022.

[59] P.A. Quinto-Su, C.-D. Ohl, Bubble cluster explosion, Phys. Fluids 22 (2010), 091109, https://doi.org/10.1063/1.3483221.